Journal of Applied Fluid Mechanics, Vol. 16, No. 7, pp. 1371-1385, 2023.
Available online at www.jafmonline.net, ISSN 1735-3572, EISSN 1735-3645.
https://doi.org/10.47176/jafm.16.07.1717

Numerical Analysis on Improving the Rectangular Texture Floating Ring Gas-film Seal Characteristics with Different Bottom Shapes

W. Shipeng, D. Xuexing†, D. Junhua and W. Jingmo

College of Petrochemical Engineering, Lanzhou University of Technology, Lanzhou, Gansu 730050, China

†*Corresponding Author Email: dingxxseal@126.com*

(Received December 13, 2022; accepted March 1, 2023)

ABSTRACT

Finding the right texture pattern to effectively improve the sealing performance of the floating ring gas film seal has always been a topic of interest for engineers. Herein, to reveal the effect of the rectangular textured base shape on the sealing characteristic parameters of floating ring gas film seal, four bottom shapes of rectangle, isosceles triangle, left triangle and right triangle were proposed. The governing equations were solved by the finite difference method and the correctness of the theoretical results was verified by the test bench. The effect of operating conditions parameters on the sealing performance were also analyzed. The results reveal that the trends of the experimental results is consistent well with the theoretical results, in which the relative errors are all less than 9%. It indicates that the theoretical model is scientific and valid. As the speed and inlet pressure increase, the texture bottom shape significantly changes the distribution of pressure and temperature field. And the average gas film thickness determines whether the texture produces an effect or not. Under the same operating conditions, a right-angled triangular bottom shape can obtain a good stability and cooling effect for the sealing device. With a bottom shape of the right triangle and a bottom shape of the rectangle, the maximum difference in opening force and gas film temperature rise were calculated to be 234.91 N and 0.61 ºC, respectively. The research results provide theoretical support for further study of the textured floating ring gas film seal and a reference for texture optimization.

Keywords: Floating ring seal; Gas lubrication; Rectangular texture; Bottom shape; Steady-state performance.

NOMENCLATURE

c_v	specific heat at constant volume	P_i	inlet pressure
C	gas properties	P_{max}	maximum gas film pressure
e	eccentricity distance	P_o	outlet pressure
F	opening force	Q	leakage rate
F_z	axial component of opening force	r	shaft sleeve radius
F_θ	circumferential component of opening force	R	shaft radius
		T	gas temperature
h_0	medium film thickness	T_i	inlet temperature
h_l	length of texture	T_0	outlet temperature
h_c	average film thickness	z	axial coordinate
h_{max}	maximum film thickness	Δh	depth of texture area
h_{min}	minimum film thickness	ΔT	temperature rise
h_t	depth of texture	Δz	step width in axial direction
L	length of floating ring	$\Delta\theta$	step width in circumferential direction
n	rotational speed	ε	eccentricity ratio
n_z	number of grids in axial direction	θ	circumferential coordinate
n_θ	number of grids in circumferential direction	μ	gas viscosity
		μ_0	medium gas viscosity value at temperature
N_z	number of axial textures	ρ	gas density
N_θ	number of circumferential textures	Ψ	attitude angle
O	center of floating ring in free state	ω	rotational angular speed of shaft
O_1	center of the rotating shaft	Ω_1	non- texture region

O_2	center of the floating ring	Ω_2	texture region
P	gas film pressure		

1. INTRODUCTION

The floating ring gas film seal is a vital functional component for preventing leakage from the shaft end of high-speed turbine compressors and are now widely used due to their energy saving and leakage prevention benefits. Most notably, sealing performance directly affects the safe operation and efficiency of rotating machinery equipment in use (Andrés and Ashton 2010; Gang *et al.* 2011). Unfortunately, there has also been some negative feedback during engineering applications. For one thing, when the hydrodynamic effect caused by the low-speed operation of the sealing device is weak, the gas film stiffness is insufficient in the seal gap. Therefore, it is difficult for the gas film force to open the stationary ring and increase the probability of friction between sealing pairs. For another thing, when the sealing device runs for a long time, the heat generated by the gas film shear force may lead to an increase in the temperature of the lubricating gas, and the thermal deformation of the sealing pairs make the sealing device failure (Xie *et al.* 2020; Sun *et al.* 2021). Due to the limited space available at the shaft end, turbo compressors are very compact. When designing the shaft end seals, how can the steady state performance be improved by effective texturing patterns without modifying the structure. The study of the above issues are of great significance to the safe operation of mechanical equipments, it has become a common concern in the research of engineering application sealing field.

Rational parameters of texture pattern can effectively improve the lubrication and anti-wear properties of the sealing surface under poor lubrication conditions (Lu *et al*. 2017). In view of this nature, there have been numerous reports on micro-texture technique applications in the field of seals and bearings. Yang *et al.* (2019) investigated the effect of the different triangle profiles distribution on the sealing performance of mechanical seals by the finite element method. They pointed out that the isosceles triangle dimples can provide a more hydrodynamic effect, and increasing the number of dimples at the inner edge helpful to reduce the leakage. Singh and Awasthi (2021) studied part of the surface textures with the aim of improving the stability performance characteristics of a journal-bearing system. By comparing the spherical, cylindrical, triangular, and kite-shaped textures bearings through calculation, they demonstrated that when the aspect ratio of the surface texture is 0.1, the spherical textures provide better stability parameters for hydrodynamic journal bearings. Shi *et al*. (2019) analyzed the influence of microgrooves and dimples patterns on mechanical seal performance and defined attribute evaluation parameters. The results demonstrate that the texture shapes with straight edges perform better than those with rounded edges. Moreover, the microgrooves with a depth of 3μm is the best choice for enhancing the sealing performance. Hu *et al*. (2019) provided a comprehensive analysis of the influence of circular textures on rotary vane actuator end-sealing performance through theoretical and experimental means. This study indicates that textured rotor surface is more likely to form hydrodynamic oil film under lubrication conditions, which can reduce the friction performance. Pei *et al*. (2016) applied the finite element method to solve the Reynolds equation and energy equation for a mathematical model of variable oil viscosity to investigate the effect of lubrication performance of smooth and textured floating ring bearings. This study suggests that the texture pattern can improve the performance of the floating ring bearings. The maximum oil film pressure was increased by 530% and the oil film temperature was reduced by 29% as compared to a smooth surface bearing.

As research into the lubricity performance of textures has intensified, texture shape optimization has also become a focus of exploration. Wang *et al.* (2018) used a genetic algorithm to numerically optimize dimples with free edges to obtain the best profile, which can generate the maximum opening force and minimum leakage. The results indicate that the optimized asymmetric “V” dimples offer better performance than other dimples with regular shapes. This work opens up the possibility of further optimizing the texture shape. Shen and Khonsari (2015) carried out a sequential quadratic programming algorithm to determine the optimal shape the optimal shape of parallel surfaces that produced the maximum load carrying capacity. The results indicate that herringbone and trapezoid are the best texture shapes under unidirectional and bidirectional sliding conditions, respectively. Wang *et al.* (2019) introduced a multi-objective optimization method to optimize texture parameters of mechanical seals and verified the optimization results through experiments. The best “free form” textures show higher opening force and lower leakage than cylindrical pits. This work offer a new avenue for further research into texture shape. Jin *et al.* (2020) designed a quadratic programming algorithm for the investigation of cylindrical crater arrangement and combination patterns with the aim of exploring and identifying the best texture arrangement mode to improve the performance of sliding bearings. By comparing the optimized texture arrangement and combination, they found that the “forward-back texture” distribution pattern could enhance the load-carrying capacity of journal-bearing. As mentioned above, scholars at home and abroad have done large numbers of research on micro-texture technology in applied engineering and have achieved fruitful results. Unfortunately, most researchers focused on numerical simulation calculations on the contour of different shapes as the research object, and the optimization of surface texture has only been limited to the optimization of

texture shape contour and algorithm. Up to now, the effect of the shape of the texture bottom on the sealing performance has been overlooked, and little research literature has been published on the subject. The resulting influence mechanism of the texture bottom shape on the sealing performance is still unclear.

In this paper, the effects of bottom shape change on the steady-state sealing performance of the floating ring gas film seal was investigated. Based on the theory of gas lubrication, four typical bottom shapes, rectangle, isosceles triangle, left triangle, and right triangle, were put forward as the study objectives. A combination of numerical analysis and experimental research methods is applied, taking into account the influence of temperature viscosity. With opening force, leakage, gas film temperature rise, and attitude angle as evaluation objectives, the influences of rotational speed, inlet pressure, and average gas film thickness on the sealing performance were simulated and analyzed. The findings of this study provide a theoretical basis for the texture structure alteration and engineering optimization of the floating ring gas film seal.

2. THEORETICAL MODEL

2.1 Geometrical Configuration

The design of the floating ring gas film seal refers to the air bearing. During the high-speed rotation of the rotating shaft, the gas on the high-pressure side will be sucked into the sealing clearance by the pump effect, resulting in hydrodynamic effects. With the increase of inlet pressure, an gas film of smaller thickness and greater stiffness appears in the seal clearance. The gas film with greater stiffness can seal the primary leakage channel and avoid collisions between rotary and stationary rings. At the same time, the use of eccentric installation between the rotating shaft and the carbon ring

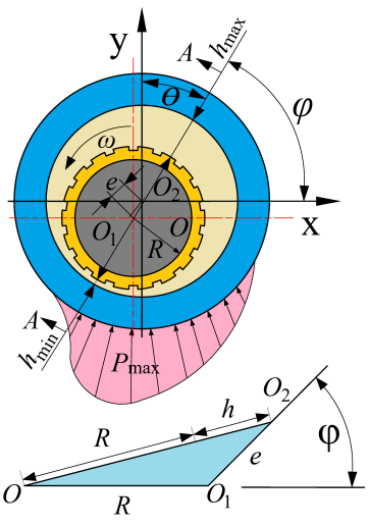

Fig. 1. Structure model of the floating ring gas film seal.

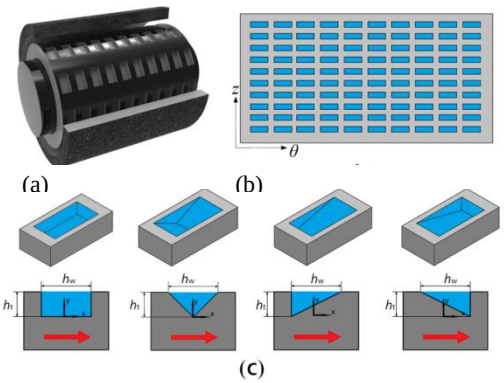

Fig. 2. Physical model of rectangular textures with different bottom shapes.

Table 1 Geometric parameters of the floating ring gas film seal

Parameters	Value
Outer radius of shaft sleeve, r (mm)	25
Texture length, h_l (mm)	13
Texture width, h_w (mm)	5
Texture depth, h_t (μm)	12
Number of axial textures, N_z	2
Number of circumferential textures, N_θ	25
Length of shaft sleeve, L (mm)	52

makes it easy to form a wedge-shaped convergent gas film space. It further enhances the hydrodynamic effect of the sealing, and consequently improves the service life of the sealing device (Joachimmiak and Krzyslak 2019; Guo *et al.* 2019). The structure model of floating ring gas film seal is shown in Fig. 1.

One of the effective ways to improve the lubrication performance of the floating ring gas film seal is to apply texture patterns to the surface of the shaft sleeve. It is worth noting that the most widely studied texture fall to the same depth. With the advancement of processing technology, scholars can carry out exaggerated designs and verification of texture shapes (Mishra *et al.* 2014; Karampour *et al.* 2021). Therefore, the study on texture bottom shapes can be seen as follows. Figure 2 depicts the geometric model of rectangular textures with different bottom shapes. The geometric parameters used in the process of numerical analysis are shown in Table 1.

2.2 Numerical solution

2.2.1 Basic Assumptions

Based on the gas lubrication theory, a thermal hydrodynamic lubrication model of the floating ring gas film seal was developed. To simplify the calculation, the following assumptions can be made during the modeling process (Lu 2020):

1. The fluid does not slip on the solid interface;
2. The surface of sealing rings is smooth and the effect of roughness is ignored.
3. The pressure and temperature of sealing gas do not change in the direction of film thickness;
4. The lubricated flow of the gas is a non-turbulent laminar flow;
5. The effect of magnetic and inertial forces are ignored.

2.2.2 Pressure Governing Equation

For a floating ring gas film seal, the compressible gas pressure distribution in cylindrical coordinates conforms to the Reynolds equation, and the following results can be obtained (Tibos *et al.* 2017) :

$$\frac{1}{r^2}\frac{\partial}{\partial\theta}\left(\frac{Ph^3}{\mu T}\frac{\partial P}{\partial\theta}\right)+\frac{\partial}{\partial z}\left(\frac{Ph^3}{\mu T}\frac{\partial P}{\partial z}\right)= 6\omega\frac{\partial}{\partial\theta}\left(\frac{Ph}{T}\right) \tag{1}$$

where r is the shaft sleeve radius, P is the gas pressure, h is to the gas film thickness, μ is the gas viscosity, T is the temperature, z is the axial coordinate, θ is the circumferential coordinate, and ω refers to the rotational angular speed of the shaft.

2.2.3 Energy Governing Equation

In order to reveal the influence of different bottom profiles of rectangular texture on the temperature rise of the gas film in the clearance, this paper considers only the energy equation in the adiabatic state at this moment, that is, only the transformation between the internal energy and the mechanical work of the gas film in the seal clearance is considered, while the energy exchange due to heat conduction between the seal pairs is overlooked. The energy equation controlling the temperature distribution of the gas film in adiabatic state can be expressed as follows (Ma *et al.* 2016) :

$$\left(\frac{h^3}{12\mu}\frac{\partial P}{r\partial\theta}-\frac{\omega rh}{2}\right)\frac{\partial T}{r\partial\theta}+\frac{h^3}{12\mu}\frac{\partial P}{\partial z}\frac{\partial T}{\partial z}= -\frac{\mu\omega^2r^2}{h\rho c_v}+\frac{h^3}{12\mu\rho c_v}\left[\left(\frac{\partial P}{r\partial\theta}\right)^2+\left(\frac{\partial P}{\partial z}\right)^2\right] \tag{2}$$

where c_v denotes specific heat at constant volume.

The effect of gas pressure on viscosity is minimal and only only the change in gas viscosity as a function of temperature (P_i<5 MPa) needs to be considered. The sutherland equation is defined as (Ma *et al.* 1981) :

$$\mu=\mu_0\left(\frac{T}{T_0}\right)^{\frac{3}{2}}\frac{(T_0+C)}{T+C} \tag{3}$$

where C represents constantly correlated with gas properties, and 124k can be taken for air and μ_0 is the corresponding lubricating gas viscosity value at temperature T_0.

2.2.4 Film Thickness Governing Equation

The h_0 is obtained by following equations (Tala-Ighil and Fillon 2015):

$$h_0=C(1+\varepsilon\cos\theta)+\Delta h(\theta,z) \tag{4}$$

For rectangular bottom shape,

$$\Delta h(\theta,z)=\begin{cases}0, & (\theta,z)\in\Omega_1\\ h_t, & (\theta,z)\in\Omega_2\end{cases} \tag{5}$$

For isosceles triangular bottom shape,

$$\Delta h(\theta,z)=\begin{cases}0, & (\theta,z)\in\Omega_1\\ -\frac{2h_t}{h_w}|X|+h_t, & (\theta,z)\in\Omega_2\end{cases} \tag{6}$$

For left triangular bottom shape,

$$\Delta h(\theta,z)=\begin{cases}0, & (\theta,z)\in\Omega_1\\ -\frac{h_t}{h_w}X+h_t, & (\theta,z)\in\Omega_2\end{cases} \tag{7}$$

For right triangular bottom shape,

$$\Delta h(\theta,z)=\begin{cases}0, & (\theta,z)\in\Omega_1\\ \frac{h_t}{h_w}X, & (\theta,z)\in\Omega_2\end{cases} \tag{8}$$

where h_0 denotes gas film thickness, Δh stands for texture depth, Ω_1 is non- texture region and Ω_2 is texture region.

2.2.5 Computation Boundary Conditions

In order to solve the pressure field and temperature fields, the following boundary conditions are set up.

1. The sealing systems using mandatory boundary conditions are as follows:

$$\begin{cases}z=0;P=P_i & z=L;P=P_o\\ z=0;T=T_i & z=L;T=T_o\end{cases} \tag{9}$$

where P_i refers to the boundary pressure at the high-pressure side, P_o is the boundary pressure at the low-pressure side and T_i and T_o represent the inlet and outlet temperatures, respectively.

2. The periodic boundary conditions for pressure and temperature with a period of 2π can be written as follows:

$$\begin{cases}P(\theta,z)=P(\theta+2\pi,z)\\ T(\theta,z)=T(\theta+2\pi,z)\end{cases} \tag{10}$$

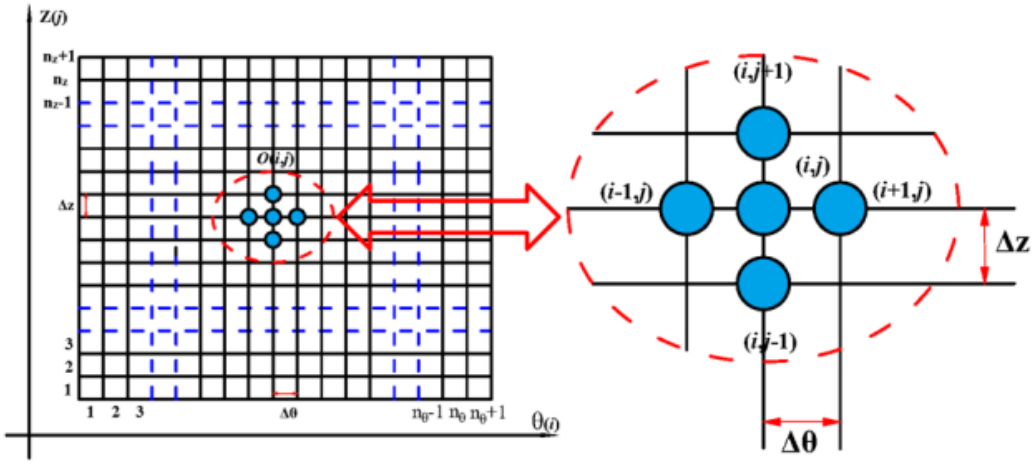

Fig. 3. Meshing of the computation domain.

2.2.6 Seal Performance Parameters

For the same number of grid nodes, the error of the central difference is smaller than that of the upwind difference. To improve the stability of the solution, the five-point central difference method in the finite difference method is applied to solve the theoretical model equations (Du and Li 2020; Hou *et al.* 2020). The calculation domain of the floating ring gas film seal was divided into n_θ and n_z along the circumferential and axial directions to obtain a solution domain of (1:n_θ+1,1:n_z+1). The axial and circumferential steps are Δz and $\Delta\theta$, respectively. The grid division of the computing domain is shown in Fig. 3.

Figure 4 shows a flow chart of the numerical solution. The iterative errors of both the pressure and temperature fields are 10^{-6}. After convergence of the iterative computation, the pressure and temperature distribution values are obtained for all nodes in the solution domain at the steady-state characteristics. To provide theoretical support for selecting the optimum bottom shape of the rectangular texture, the steady-state sealing performance of floating ring gas film seals with different bottom shapes was calculated. In addition, gas film temperature rise and attitude angle were analyzed to further evaluate the benefits of different bottom types. Among them, the gas film temperature rise represents the heat dissipation performance of the shaft sleeve. The lower the gas film temperature rises, the better the heat dissipation effect is. The attitude angle represents the stability of the sealing prototype and the smaller the attitude angle is, the more stable the sealing structure is (Chen *et al.* 2020).

1. The gas film opening force F can be expressed as follows:

$$\begin{cases} F_z = r\int_0^L\int_0^{2\pi} P\cos\theta d\theta dz \\ F_\theta = r\int_0^L\int_0^{2\pi} P\sin\theta d\theta dz \\ F = \left(F_z^2 + F_\theta^2\right)^{1/2} \end{cases} \tag{11}$$

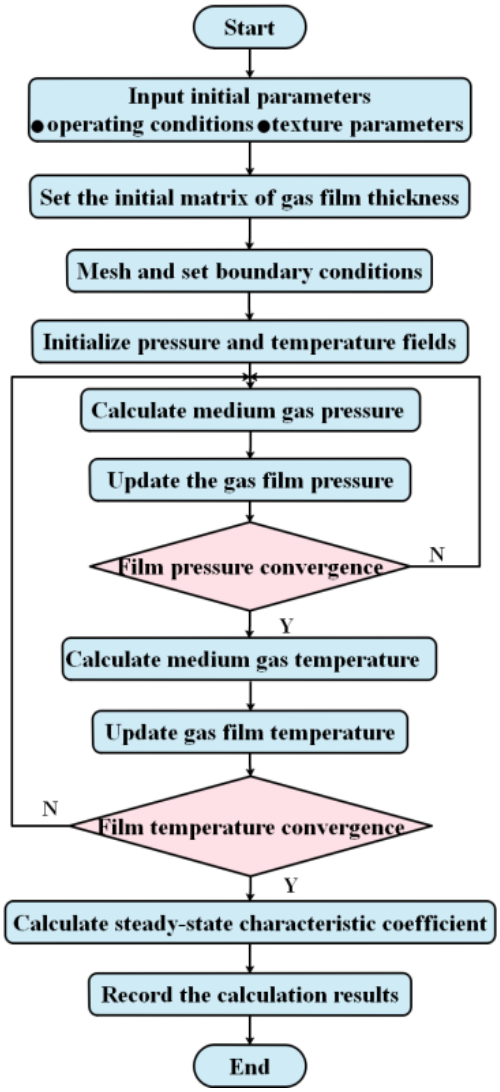

Fig. 4. Numerical calculation flow chart of floating ring gas film seal.

where F_z and F_θ denote the axial and circumferential gas film opening force components, respectively, and F is total gas film opening force.

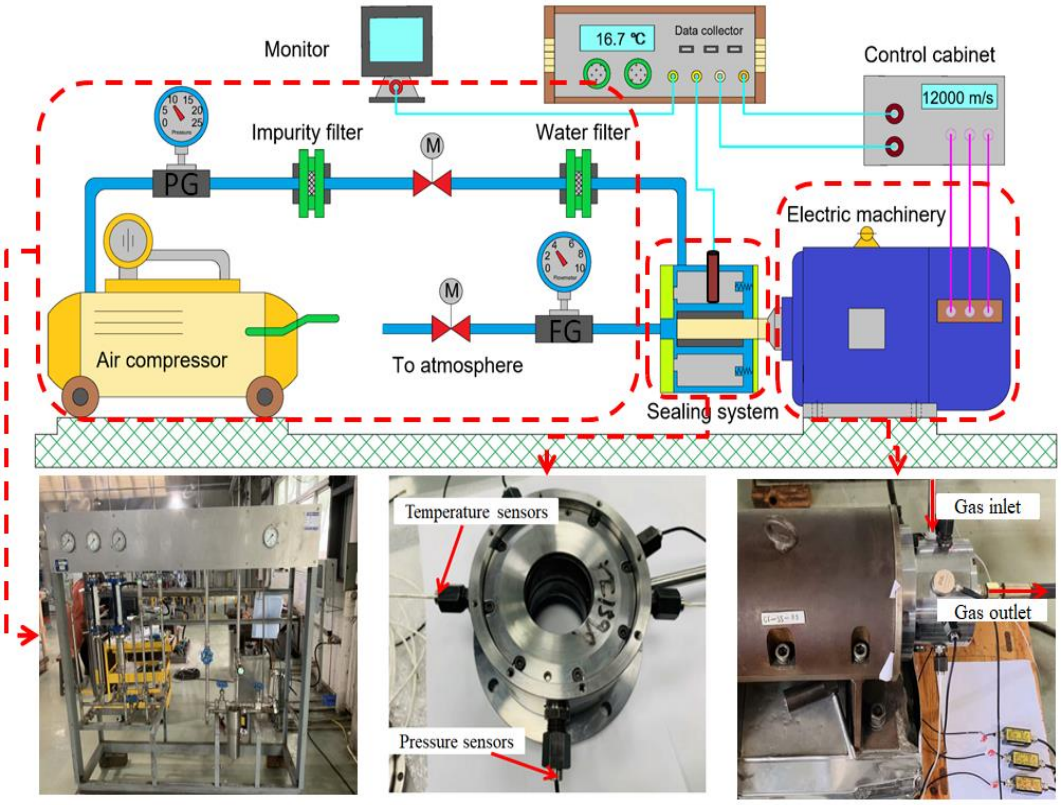

Fig. 5. Test rig of floating ring gas film seal.

2. The gas leakage rate Q can be expressed as follows:

$$Q = r\int_0^{2\pi}\left(-\frac{h^3}{12\eta}\frac{\partial p}{\partial z}\right)\rho d\theta \tag{12}$$

3. The attitude angle Ψ can be expressed as follows:

$$\psi = \tan^{-1}\left(F_\theta / F_z\right) \tag{13}$$

3. EXPERIMENTAL TEST

3.1 Experimental Apparatus

In constructing the test rig of the floating ring gas film seal, the design methods of air bearing and mechanical seal test system were adopted as guidelines (Wang *et al*. 2014). In order to fully and clearly present the test bench, the specific physical connection of the test bench is shown in Fig. 5. The test contains the leakage per unit time of the seal system and the gas film temperature rise of the sealing prototype at different operating parameters. The test data obtained is transmitted to the computer for screening processing and storage via a multi-channel high-frequency data collector. Through analysis and discussion, the influence rule of sealing performance of floating ring sealing device under different working conditions, and feedback to the theoretical model for correction, providing guidance and suggestions for the design and optimisation of the texture pattern of the floating ring gas film seal.

3.2 Measuring Technique

3.2.1 Measuring Technique of Leakage

Leakage rate is an essential index to evaluate the performance of a sealing prototype, so accurate measurement of leakage per unit of time has important guiding significance for the design and optimization of the gas film seal system. It is noteworthy that the leakage value of the sealing device is small as calculated by simulation. The sensitivity of the leak measurement apparatus normally used is not sufficient to meet the accuracy requirements of the test. A metal tube float flowmeter suitable for small pipe diameter, low flow rate, and high-pressure resistance was selected to obtain the accurate leakage of lubricating gas in this test. The model is H250, and its measuring accuracy can reach 0.05m^3/h.

3.2.2 Measuring Technique of Temperature

The gas film temperature test is carried out based on the steady operation of sealing prototype. To ensure that the temperature sensors does not damage the gas film and timely senses the gas film temperature during the detection process, two non-penetrating holes are machined in the outer surface of the carbon ring. Notably, the distance between the bottom of the hole and the inner surface of the carbon ring does not exceed 0.5mm. The two sensors are included at an angle of 180°, with axial positions corresponding to the middle and edge of the shaft sleeve, respectively. The main reason for

this arrangement is to prevent localized high temperature that could cause damage to the test sensors arranged on the carbon ring surface. The temperature sensors are dual-channel intelligent temperature transmitters. The sensor is a thermal resistance Pt100, which converts the measured data into voltage signals and imports the MPS-140801-U acquisition card. The acquisition card converts and amplifies the received signals and then displays the temperature on the computer screen.

3.3 Anti-Jamming Measure

Considering that other sealing prototypes were installed in the test workshop, the vibrations and noise they generates might interfere with the test system during operation. Due to the high sensitivity of the selected sensors, the following anti-signal interference measures were adopted for the test bench to ensure the accuracy of the test values (Zhang *et al*. 2011; Abuelma'atti and Abuelmaatti 2013):

(1) The motor and the instrument power supplies are connected separately to reduce the interference caused by the power supply itself or abnormal power jitter;

(2) The signal lines are kept as far away from the powerful electric current lines as possible to reduce the mutual inductance and magnetic field coupling interference;

(3) The instrument and equipment are protected by a conductive cartridge made of metal material and shielded from associated electric fields.

3.4 Preparation of Specimens

In the test, the rotating and stationary rings were made from carborundum and graphite respectively. The relatively soft graphite material was selected as the static ring to facilitate the processing of the temperature measurement hole. Due to the low opening force of the gas film seal during start-stop, the sealing pairs are likely to friction. Considering that the rectangular micro-texture depth proposed in this study was in the micron range, the seal performance was affected by the change in gas film thickness in order to prevent the micro-texture from being worn or covered by graphite chips. So, the carborundum was used as the rotating ring with rectangular textures on the surface. Figure 6 displays the physical pictures of the seal pairs.

4. VALIDATION

The design and safe operation of high-performance turbine machinery requires accurate prediction of sealing performance generated by floating ring gas film seal. In order to select the best rectangular texture, the steady-state performance parameters were calculated for the rectangular texture floating ring gas film seal with different bottom shapes and reveal its sealing mechanism. Table 2 lists the operating parameters in the current study.

(a) rotary ring (b) stationary ring

Fig. 6. Specimens of rotary and stationary rings.

Table 2 Working condition of the floating ring gas film seal.

Parameters	Value
Average gas film thickness, h_c (μm)	5
Inlet pressure, P_i (MPa)	0.8
Outlet pressure, P_0 (MPa)	0.101
Viscosity, μ(Pa.s)	1.8×10^{-5}
Rotational speed, n(krpm)	13
Eccentricity, ε	0.7
Inlet temperature, T_i(°C)	25
Density, ρ(kg/m^3)	1.1452

4.1 Theoretical Calculation

The results of calculation can be demonstrated in Fig. 7, where the gas film thickness, the gas film pressure, and the gas film temperature distribution of the rectangular texture floating ring sealing with different bottom shapes are presented. As shown in Fig. 7(a), the rectangular textures with different bottom shapes are orderly arranged on the shaft sleeve surface. As a result of the existence of eccentricity, the gas film thickness distribution within the sealing clearance has an overall parabolic shape. Among them, the lowest point and the highest point are represented the thinnest and thickness of the gas film thickness, respectively. The height of the raised regular contour is the depth of the rectangular textures with different bottom shapes. The lubricating gas in the wedge clearance rotates with the shaft sleeve at high speed, creating a hydrodynamic effect that separates the carbon ring from the shaft sleeve and enables non-contact operation of the sealing pairs.

According to Fig. 7(b), in the axial direction, the inlet pressure distribution presents a distribution trend of increasing and then decreasing. In the circumferential direction, hydrodynamic effect can be generated in the area with the thinnest film thickness, which belongs to the pressurized areas. As a result of the existence of surface textures, there are micro-scale steps at the junction of texture and non-texture areas. During the axial flow, gas passes alternately through the two regions. The change of the gas volume in the texture holes area and the collision of gas molecules at the boundary of the micro-texture hole cause the gas film pressure to

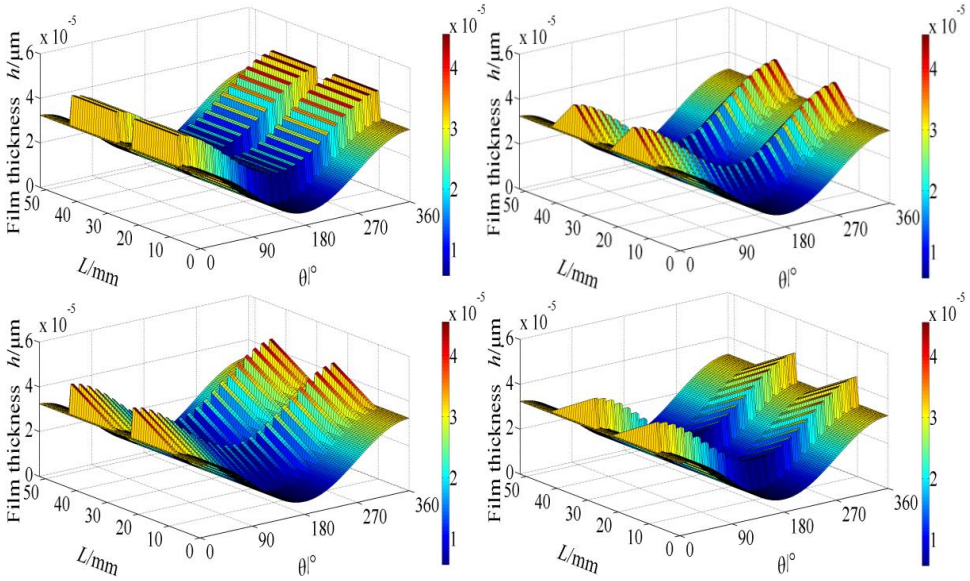

(a) gas film thickness distribution

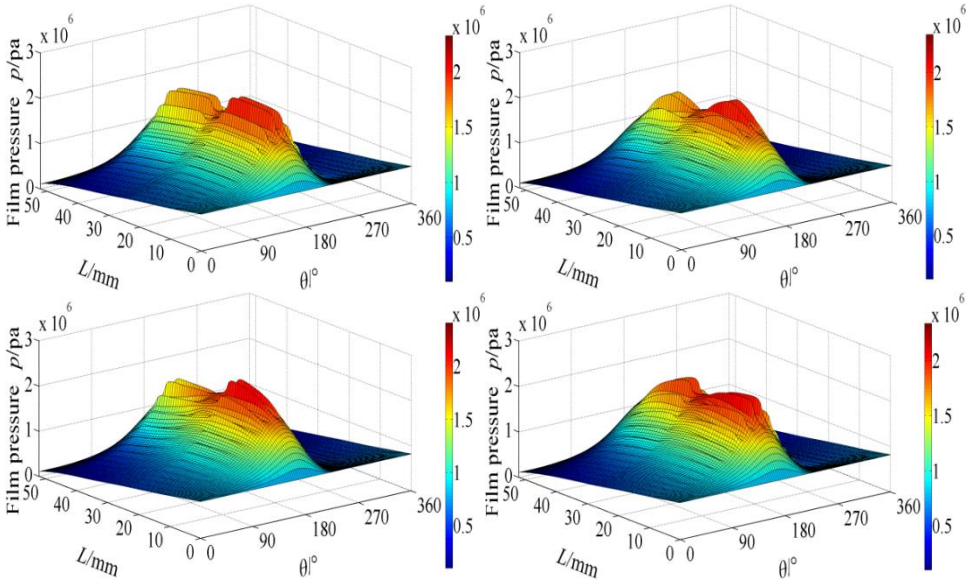

(b) gas film pressure distribution

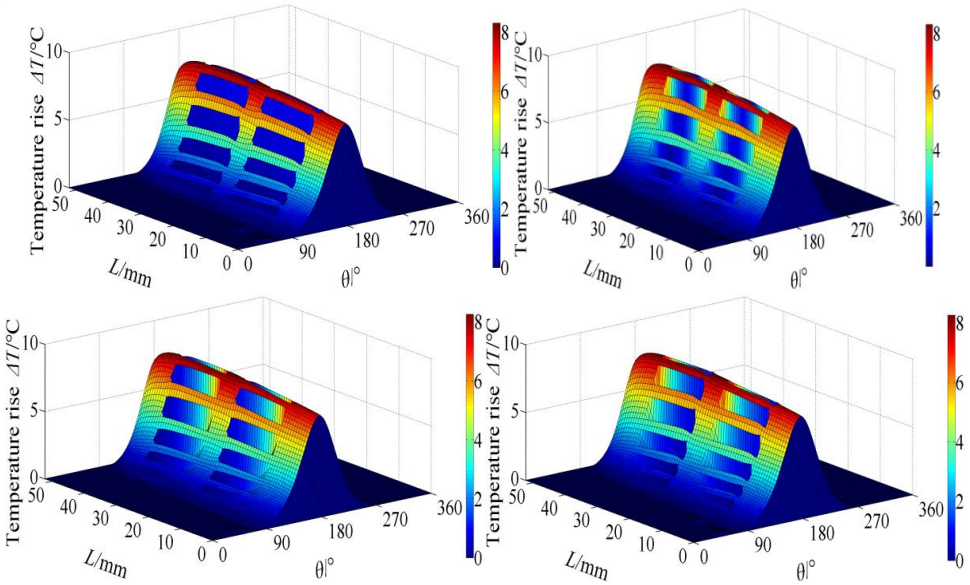

(c) gas film temperature rise distribution

Fig. 7. Simulation results of flow field of floating ring gas film seal.

fluctuate to a certain extent here. Pressure peaks are generated at the end of each pit control unit, resulting in the maximum gas film pressure in the axial direction changing from a smooth curve to a saw tooth curve. This is the reason why the general distribution of gas film pressure is sawtooth shaped. Notably, different bottom shapes of rectangular texture holes are produced different hydrodynamic effects.

Figure 7(c) displays that the gas film temperature rise distribution is influenced by the combined action of shear flow and pressure flow in the sealing clearance. The pressure flow of the radial sealing causes the gas film temperature to rise gradually along the direction of leakage, while the shear flow in the circumferential velocity causes the gas film temperature to rise. It is worth mentioning that the highest gas film temperature rise occurs where the gas film thickness is the thinnest. The dented part of the picture is the rectangular textures with different bottom shapes. Due to the low gas viscosity, the gas film thickness in the existing texture region is large, and the gas film temperature rise value with heavily different.

Based on the above presentation of the gas film thickness, inlet pressure and gas film temperature rise distribution of floating ring gas film seal, the results reveal that different texture shapes have unlike effects on sealing performance. Therefore, in the following sections, the steady-state characteristic parameters of the rectangular texture with four kinds of diverse bottom profiles are systematically studied to obtain the optimum texture parameters.

4.2 Test Verification

In order to accurately predict the sealing performance of the rectangular texture with different bottom profiles of the floating ring gas film seal, it is necessary to verify the correctness of mathematical model and to check the validity of the computer code. In this test, inlet pressures of 0.3 MPa to 1 MPa were chosen to test the steady-state characteristic parameters of floating ring gas film seal. Significantly, the rotating speed was set to 12000 r/min and 16000 r/min, respectively. During stable operation, the sealing prototype test content contains the leakage amount per unit of time and the gas film temperature rise.

Figure 8(a) and 8(b) present the variation of leakage by inlet pressure. When observing the above figures, the leakage of the test results is slightly higher than the theoretical calculation. Both the theoretical and experimental results show an increasing trend in leakage with increasing inlet pressure. This is mainly due to the rise in pressure resulting in an increase in the differential pressure of the lubricating gas. As a result, the axial gas flow volume is increased in the sealing device, resulting in an increase in flow rate and a sharp rise in leakage. Notably, the leakage volume decreases with increasing speed In addition, when the rotational speed is 12000 r/min, the maximum relative error is 8.6% at 0.7 MPa. The minimum relative error is 3.4% at 0.3 MPa. For the rotational speed of 16000r/min, the maximum error is 7.9% at 0.6 MPa. The minimum error is 4.1% at 0.3 MPa. The calculated results agree well with the experimental values. The maximum relative error is

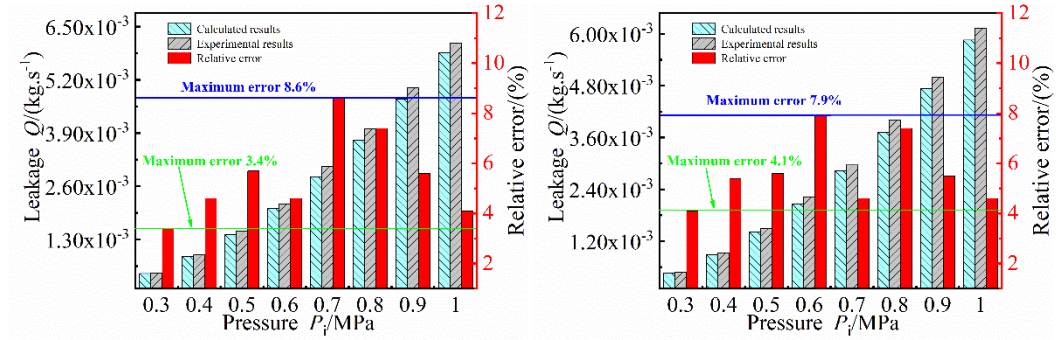

(a) leakage (n=12000r/min) (b) leakage (n=16000r/min)

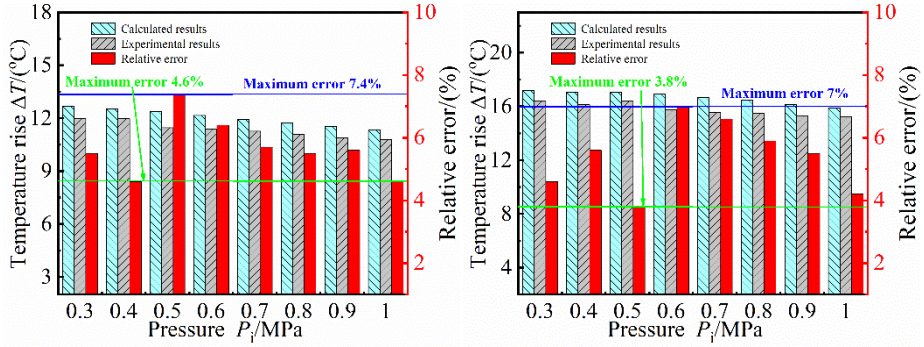

(c) temperature rise (n=12000r/m) (d) temperature rise (n=16000r/min)

Fig. 8. Distribution of the experimental and calculated values of the floating ring gas film seal.

less than 9% in this section, which demonstrates the validity of the mathematical model in this paper.

Figures 8(c) and 8(d) reveal the variation of the gas film temperature rise with inlet pressure. As indicated by the above figures, the gas film temperature rise of the test results is slightly lower than the theoretical calculation. Both theoretical and experimental results reveal that the gas film temperature rise decreases with inlet pressure increasing. The main reason for this is that the pressure difference of sealing gas increases with the increase of pressure. As a result, it accelerates the flow of sealing gas to the low-pressure side, and the heat generated in the seal gap flows into the air with leakage gas. It effectively inhibits the temperature rise of sealing gas. It is worth mentioning that the gas film temperature rise increases with increasing of rotational speed. At a speed of 12000 r/min, the gas film temperature rise decreases slightly by 1.36 ^{o}C with the increase of pressure, with a maximum relative error of 7.4% at 0.5 MPa. The minimum relative error is 4.6% at 0.4 MPa. For a speed of 16000 r/min, the gas film temperature rise decreases slightly by 1.32 ^{o}C with the pressure increasing, with a maximum error of 7% at 0.6 MPa. The minimum error is 3.8% at 0.5 MPa. The calculated results are in good agreement with the experimental values. In this study, the maximum relative error of the gas film temperature rise is less than 8%, which further verifies the accuracy of the computation method and process of the coupling of pressure and temperature.

The numerical simulation results of the sealing prototype are consistent with the experimental results, but there are still some relative errors between the two. The main reasons for the relative error are as follows. On the one hand, the theoretical model did not consider the installation error and deformation factors, resulting in a slightly higher test leakage than the calculated results. On the other hand, due to the compact construction of the sealing device, it is impossible to arrange more temperature sensors on the shaft sleeve surface. As a result, the limited number of sensors could not measure the changes in temperature across the gas film with complete accuracy. There are relative errors, but the maximum relative error is less than 9%. This proves the scientific validity of the theoretical model and the applicability of the calculation code.

5. RESULTS AND DISCUSSION

The purpose is to study the influence of the steady-state characteristic parameters of rectangular textured floating ring gas film seals with different bottom surface shapes at different speeds, inlet pressures and average gas film thicknesses. The simulation parameters used for numerical computation are listed in Tables 1 and 2.

5.1 Influence on Rotational Speed

Figure 9 shows the curves of of the variation of the numerical results variation of sealing performance for different bottom shapes of rectangular textures at varying rotational speeds. As can be seen in Fig. 9(a), the opening forces generated by texture holes with four kinds of bottom profiles all show an upward trend with the rotational speed increasing. Moreover, the higher the rotational speed, the more significant the generated hydrodynamic effect capacity of the rectangular textured pattern, and the higher the value gap of opening force between the four kinds of bottom shapes. At a speed of 14000 r/min, the maximum different value gap between the opening forces by the bottom of the right triangle and rectangular is 234.91 N. Further observation reveals that the opening forces of the rectangular are lower than the other three bottom types. The main reason for this is the increasing speed of rotation, where the rectangular textures gradually comes into play. The gas undergoes an alternating cycle of instantaneous compression and expansion in the discrete texture dimples, and the significant hydrodynamic effect generated by the shaft sleeve surface enhances to achieve the sealing capacity. However, the ability to generate significant hydrodynamic effect varies due to the bottom shape of the rectangular texture. The higher the rotational speed, the higher the difference value gap of the opening force.

As shown in Fig. 9(b), the amount of leakage generated by the texture dimples of the four kinds of bottom profiles shows a slight downward trend with increasing rotational speed. Among them, the rectangle bottom drops by 1.38×10^{-5} kg.s^{-1}, the isosceles triangle bottom falls by 1.63×10^{-6} kg.s^{-1}, the left triangle bottom drops by 5.01×10^{-6} kg.s^{-1}, and the right triangle bottom falls by 4.11×10^{-6} kg.s^{-1}. These trends are mainly due to the enhanced hydrodynamic effect in the sealing gap with rotational speed increasing. The stronger the blocking effect of rectangular texture holes on lubricating gas, the more sealing performance is effectively improved. Leakage varies considerably due to the different volume proportions of the bottom profile of the different textures. Therefore, when the rotational speed increases, the leakage volume decreases to a limited extent. In addition, the leakage rate of texture holes with different profiles is significantly different.

Figure 9(c) shows the variation curves of the gas film temperature rise with rotational speed. As shown, the temperature rise of the gas film for the different shapes of the rectangular bottom increased linearly with increasing speed. Among them, the rectangular bottom rises by 6.81 ^{o}C, the isosceles triangle bottom increases by 6.46 ^{o}C, the right triangular bottom rises by 6.66 ^{o}C, and the left triangular bottom increases by 6.28 ^{o}C. Further observation demonstrates that there is little difference in gas film temperature rise as the rotating speed increases, with the maximum different value gap between the gas film temperature rise by the bottom of the right triangle and rectangular being 0.61 ^{o}C. For the gas film temperature, the higher the rotational speed is, the greater the shear force is. Notably,t the

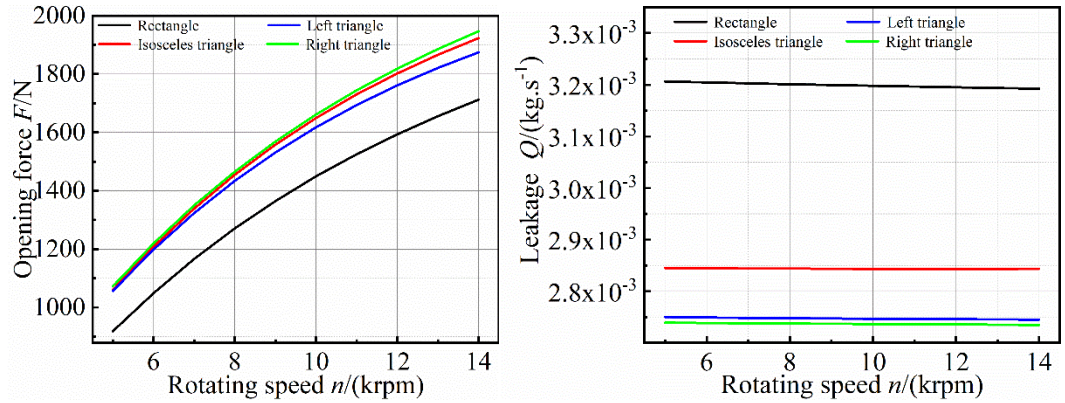

(a) opening force (b) leakage

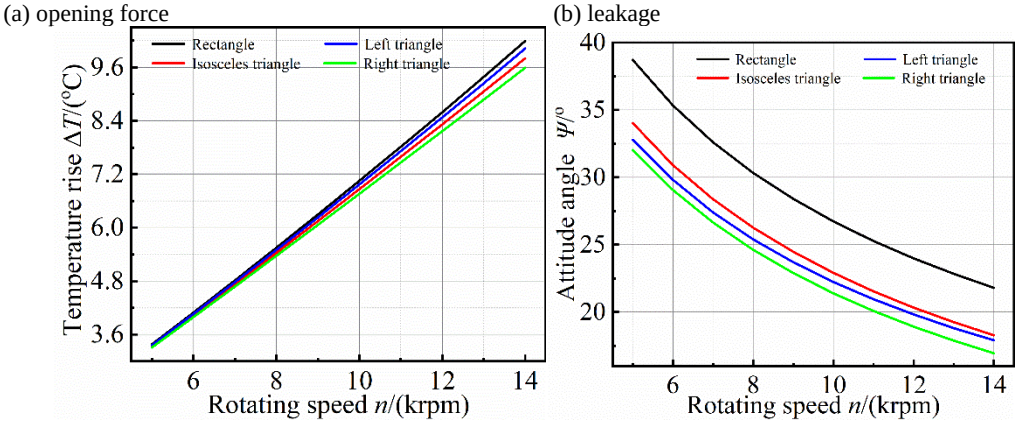

(c) temperature rise (d) attitude angle

Fig. 9. Influence of rotational speed on sealing performance.

circumferential velocity shear flow is the main factor contributing to the rise in gas film temperature.

Figure 9(d) shows the effect of the attitude angle with rotational speed. As can be observed, the attitude angle of rectangular texture with different bottom shapes decreases obviously with the rotational speed increase. However, a closer look reveals that attitude angle of the rectangular texture with different bottom shapes is higher than the other three bottom types when the rotational speed is increased from 5000 r/min to 14000 r/min. Notably, the smaller attitude angle can make the sealing prototype work more stable, which also proves that the floating ring gas film seal is more suitable for high-speed working conditions. Therefore, a rectangular micro-texture with the right triangular bottom shape may be the best choice to improve the performance of the sealing device under high-speed conditions.

5.2 Influence on Sealing Pressure

Figure 10 shows the numerical results variation curve of sealing performance of rectangular texture with different bottom shapes for varying inlet pressures. As can be seen in Fig. 10(a), all four bottom shapes of the textured holes produce an increasing trend in opening force with increasing inlet pressure. Compared with the other three bottom types, the rectangular bottom has the worst ability to enhance the hydrodynamic effect. The difference in opening forces between the right triangular and rectangular bottoms is 300.77 N at a pressure of 1.2 MPa. The main reason is that the additional hydrodynamic effect of the formation of texture dimples is not isolated, but rather the gas film pressure generation and interaction between the rectangular texture dimples are arranged based on some rules. In addition, the superposition of hydrodynamic effects increases the opening force in the sealing clearance. The hydrodynamic effect generated by the texture holes has little influence on the whole pressure distribution peak. Therefore, the opening force increases almost linearly with the increase of the inlet pressure, but for rectangular texture with different bottom shapes, the difference in values of the opening force is small.

Figure 10(b) shows the influence of leakage with pressure. It can be seen from the observation figure that when the inlet pressure is low, the value difference gap in the leakage of the texture dimples with different geometric profiles is small, and the leakage increases with the increasing pressure. Among them, the rectangle bottom increases by 6.86×10^{-3} kg.s^{-1}, the isosceles triangle bottom rises by 6.09×10^{-3} kg.s^{-1}, the left triangle bottom increases by 5.88×10^{-3} kg.s^{-1}, and the right triangle bottom rises by 5.86×10^{-3} kg.s^{-1}. The main reason is that the gas viscosity is low, and the hydrodynamic effect generated by the circumferential shear flow is far less than the hydrostatic pressure. Generally, the gas static pressure supplied by the inlet pressure plays a dominant role in sealing clearance.

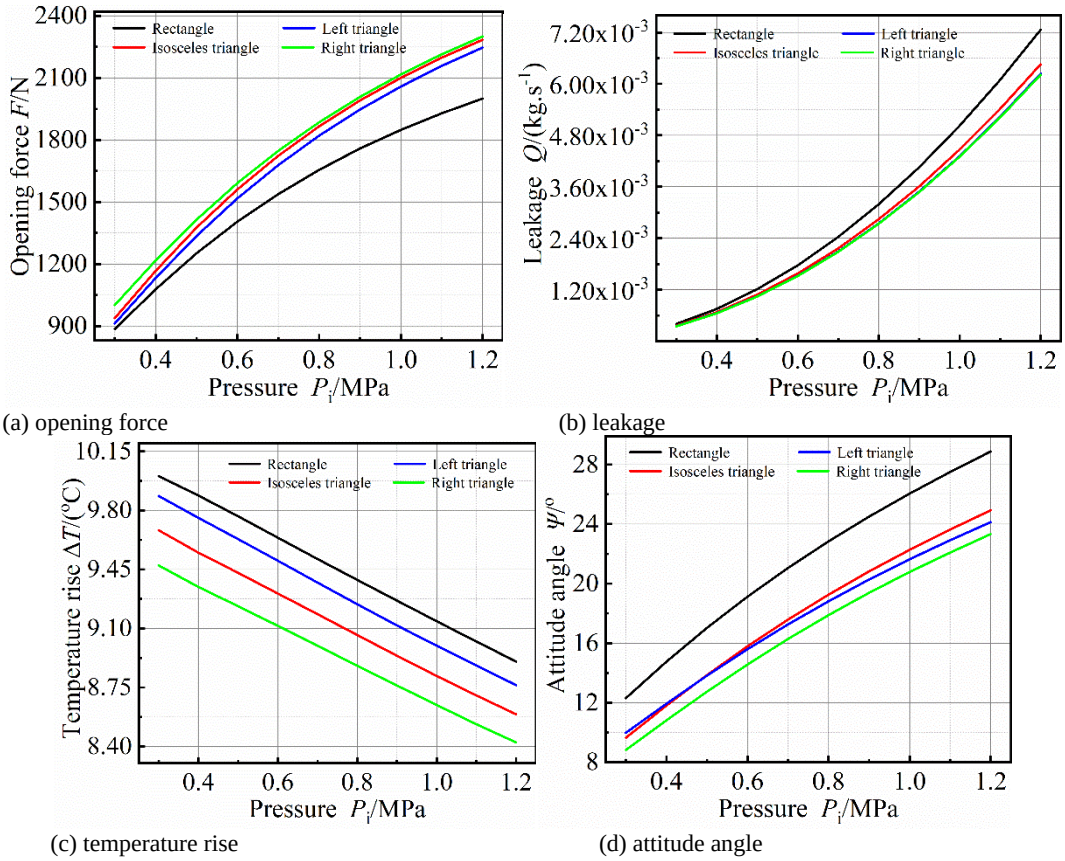

(a) opening force (b) leakage

(c) temperature rise (d) attitude angle

Fig. 10. Influence of sealing pressure on sealing performance.

Interestingly,an increase in inlet pressure leads to an increase in the value of the differential pressure of the lubricating gas. The pressure difference is the chief factor to result in the gas flow velocity increase under the axial direction and leads to the leakage increasing quickly per unit of time. However, due to the existence of rectangular textures at different bottoms, the flow rate of lubrication gas in the area of the texture holes decreases, and the leakage also changes. It can therefore be deduced that the influence of inlet pressure change on leakage is more than that of rotational speed.

Figure 10(c) shows the effect of rising gas film temperature with pressure. As the graph shows, the gas film temperature decreases linearly with the increase of inlet pressure. The larger the pressure difference gap is, the lower the value of the gas film temperature rise is. For the gas film temperature rise, within the range of the film pressure discussed, the rectangular bottom drops by 2.40 ºC, the isosceles triangle bottom falls by 2.37 ºC, the left triangle bottom drops by 2.49 ºC, and the right triangle bottom falls by 2.47 ºC. The primary reason for these trends is that when the rotational speed remains constant, the pressure flow formed by sealing pressure plays a dominant role. When the inlet pressure is increased, the pressure gradient is enhanced, accelerating the flow of medium gas to the atmospheric side and leads to the leakage enlarge. At the same time, the heat generated flows into the air with the leaking gas, effectively suppressing the rise in temperature of the gas film in the sealing gap.

Figure 10(d) demonstrates the impact of the attitude angle with pressure. As shown in the figure, the attitude angle increases linearly with the increase of inlet pressure, which is different from the law that the attitude angle decreases with the rotational speed increase in Fig. 9 (d). Further observation reveals that when the inlet pressure is below 0.5 MPa, the numerical order of the attitude angle is bottom of rectangle>left triangle>isosceles triangle>right triangle. When the gas pressure is above 0.5 MPa, the numerical order of the attitude angle is bottom of rectangle> isosceles triangle >left triangle >right triangle. The major reason for this is that the increase in pressure corresponds to a rise in the value of the floating ring load, resulting in the attitude angle increase and the stability of the sealing device decrease. Therefore, it can be deduced that the floating ring gas film seal is more suitable under low-pressure conditions, and the rectangle texture with the right triangle bottom shape may be the optimum choice to improve the performance of the sealing device.

5.3 Influence on Average Film Thickness

Figure 11 shows the numerical results variation curve of sealing performance of rectangular texture with different bottom shapes under varying average gas film thickness. As indicated in Fig. 11(a), the

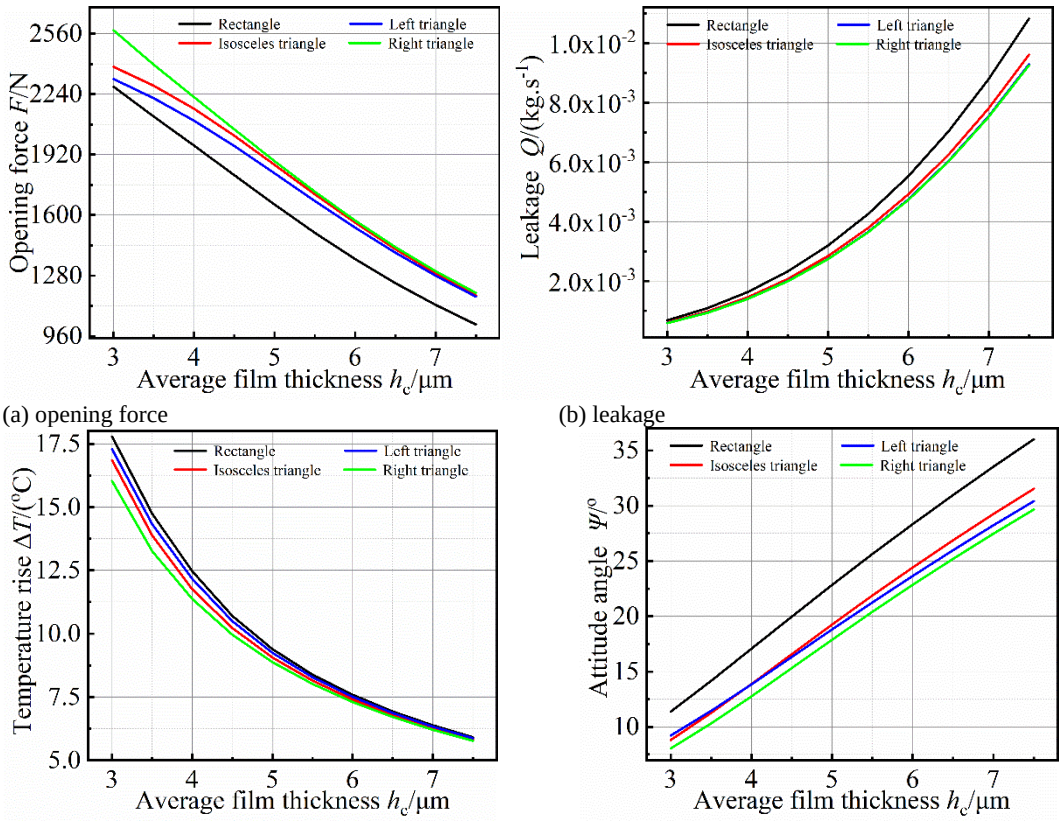

(a) opening force (b) leakage

(c) temperature rise (d) attitude angle

Fig. 11. Influence of average film thickness on sealing performance.

opening forces generated by texture holes with four kinds of bottom profiles all display decreasing trend with average gas film thickness increases. This shows that the effect of the average gas film thickness on the opening force quite obvious. It can be further observed that when the gas film thickness increases to about 7μm, the opening forces generated by the four types of bottoms have almost no difference. The primary reason for this is that when the gas film thickness is small, the thinnest film thickness is squeezed, which strengthens the wedge effect. Due to the rectangular texture on the surface of the shaft sleeve, the hydrodynamic effect is also enhanced in the thinnest region of the gas film. As a result, the opening force increases significantly, which confirms that the gas film thickness is the crucial parameter limiting whether the texture exerts a hydrodynamic effect. When the gas film thickness rises, this leads to an increase in the circumferential clearance, making it difficult to form a convergence clearance in the sealing prototype and consequently resulting in a linear decline in the opening force.

Figure 11(b) shows the effect of leakage as a function of average gas film thickness. As observed in the figure, the leakage different shapes of rectangular textured dimples increases significantly with increasing average gas film thickness. Further observation demonstrates that four types of bottom shapes produce leakage by the average gas film thickness rising gradually, with the rectangular bottom shape of the rectangular texture performing the worst. When the average gas film thickness increases from 3μm to 7.5μm, the leakage increases by 1.01×10^{-2}kg.s^{-1} for the rectangular bottom, 8.98×10^{-3} kg.s^{-1} for the isosceles triangle, 8.68×10^{-3} kg.s^{-1} for the left triangle and 8.65×10^{-3} kg.s^{-1} for the right triangle. The primary reason for this is that the increase in minimum gas film thickness lowers the change of pressure gradient in the circumferential sealing gap, decreasing the ability to generate local gas film high-pressure, and the ability to control leakage. In addition, the blocking effect of texture on lubricating gas is weakened with the average gas film thickness increase, so the leakage value increases.

Figure 11(c) shows the influence of gas film temperature rise with average gas film thickness. As can be seen from the figure, the gas film temperature rise declined with the increase in average gas film thickness. When the thickness of the gas film is increased to 6.5μm, the four bottom shapes have almost the same capability to reduce the temperature of the gas film. Among them, the rectangle bottom decreases by 66.75%, the isosceles triangle bottom falls by 65.44%, the left triangle bottom decreases by 65.85%, and the right triangle bottom falls by 63.97%. The four different types of rectangle texture dimples gradually do not function as compared to the increased opening force. The main reason for this is that, due to the small thickness of the gas film, the lubricating gas is easily squeezed by the rotating shaft in the sealing gap and the medium gas collides with the pore wall of the textured micro-pore domain. Due to the barrier of the wall, kinetic energy is transformed

into pressure potential energy instantly and the pressure of the local gas film rises rapidly. However, the gas film thickness is modified, and the friction heat generated decreases as the average gas film thickness increases. As a result, the flow rate increases in the sealing gap, and the friction heat releases into the air with the leaking lubricating gas.

Figure 11(d) shows the impact of the attitude angle with average gas film thickness. When the average gas film thickness of increases from 3μm to 7.5μm, the attitude angle of different bottom profiles all display upward trends. This indirectly indicates that the stability of the sealing device is decreasing. Further observation reveals that the stability order of the isosceles triangle and left triangle changes before and after the turning point when the average gas film thickness is 4μm. Notably, the attitude angle of the right triangle bottom shape is always the lowest, compared with the other three types of bottom profile. The major reason for this is that the gas film stiffness decreases with the gas film thickness increase, and the attitude angle, which represents the stability of the seal, increases. This suggests that the gas film thickness restricts the function of the texture rectangle. As a result, the right triangle once again proves to be more suitable in terms of stability.

6. CONCLUSION

In this paper, the correctness of the mathematical model considering the bottom shapes of rectangular textures was verified experimentally. Based on the verified theoretical model, the effect of four types of bottom shapes on the steady-state characteristics of the floating ring gas film seal was discussed with the operating condition changed. The conclusions are presented below:

- The variation trends of the experimental results are consistent with the theoretical results, and the relative errors are all less than 9%, which indicates that the theoretical model is scientifically valid. Moreover, the texture's bottom shape leads to the pressure and temperature field distribution changing significantly, which cannot be neglected when improving the structure of the sealing system.
- For the four bottom shapes proposed by rectangular texture, the opening force increases with increasing rotational speed and pressure. However, the opening forces decrease significantly with increasing average gas film thickness. The leakage increases remarkably with increasing pressure and average gas film thickness and changes slightly with increasing rotational speed.
- Four types of bottom shapes were evaluated combined with the effect of the gas film temperature rise and attitude angle. To obtain good sealing performance in engineering applications, the texture bottom shape can be selected in the order of right triangle, left triangle, isosceles triangle, and rectangle.
- For the textured floating ring gas film seal, it is necessary to consider the influence of texture region roughness on the pressure field distribution to improve the application range of the model.

ACKNOWLEDGEMENTS

This work was co-supported by the National Natural Science Foundation of China (Grant No. 51565029) and the National Key R&D Program of China (Grant No. 2020YFB2010000).

REFERENCES

Abuelma'atti, M. T. and A. M. Abuelmaatti (2013). Effect of electromagnetic interference (EMI) on the DC shift, harmonic, and intermodulation performance of NMOSFET mirror with a capacitor between the mirror node and the ground. *IEEE Transactions on Electromagnetic Compatibility* 55(5), 849-854.

Andrés, L. and Z. Ashton (2010). Comparison of leakage performance in three types of gas annular seals operating at a high temperature (300ºC). *Tribology Transactions* 53(3), 463-471.

Chen, X., J. K. Mills and G. Bao (2020). Static performance of the aerostatic journal bearing with grooves. *Proceedings of the Institution of Mechanical Engineers, Part J: Journal of Engineering Tribology* 234(7), 1114-1130.

Du, Y. and M. Li (2020). Effects on lubrication characteristics of water-lubricated rubber bearings with journal tilting and surface roughness. *Proceedings of the Institution of Mechanical Engineers, Part J: Journal of Engineering Tribology* 234(2), 161-171.

Gang, M., Z. Wei and X. Shen (2011). Analysis of Parameters and performance for spiral grooved cylindrical gas film seal. *Procedia Engineering* 23(5), 115-119.

Guo, H., S. Yang and S. Zhang (2019). Influence of temperature–viscosity effect on ring-journal speed ratio and stability for a hydrodynamic floating ring bearing. *Industrial Lubrication & Tribology* 71(4), 540-547.

Hou, G., H. Su and G. Chen (2020). Performance analysis of compliant cylindrical intershaft seal. *Science Progress* 103(3), 01-24.

Hu, T., L. Xie and J. Liu (2019). Effects of rotor surface texture on rotary vane actuator end sealing performance. *Tribology International* 140, 1058-1068.

Jin, J., X. Chen and Y. Fu (2020). Optimal design of the slip-texture on a journal-bearing surface. *Industrial Lubrication and Tribology* 73(2), 230-237.

Joachimmiak, D. and P. Krzyslak (2019). Analysis of the gas flow in a labyrinth seal of variable

pitch . *Journal of Applied Fluid Mechanics* 12(3), 921-930.

Karampour, H., Z. Wu and M. S. Mason (2021). An experimental investigation of forces on a textured cylinder at subcritical reynolds numbers. *Journal of Applied Fluid Mechanics* 14(6), 1787-1793.

Lu, J. (2020). Theoretical optimization and experiment on lubrication of floating microgroove cylindrical seal. *Industrial Lubrication and Tribology* 72(10), 1217-1226.

Lu, P., R. J. Wood and M. G. Gee (2017). The use of anisotropic texturing for control of directional friction. *Tribology International* 113, 169-181.

Ma, C., S. Bai and X. Peng (2016). Thermo-hydrodynamic characteristics of spiral groove gas face seals operating at low pressure. *Tribology International* 95, 44-54.

Ma, P., B. Jiang and J. Zhang (1981). Critical assessment of viscosity and its correlation with temperature for gaseous substances under normal pressure. *Journal of Chemical Industry and Engineering* 32(3), 193-205. (in Chinese).

Mishra, S., A. Choudhury and S. Sahu (2014). CFD investigation of influences of reverse textures on bearing surface of a journal bearing. *Journal of Applied Fluid Mechanics* 7(3), 395-399.

Pei, S., H. Xu and M. Yun (2016). Effects of surface texture on the lubrication performance of the floating ring bearing. *Tribology International* 102, 143-153.

Shen, C. and M. M. Khonsari (2015). Numerical optimization of texture shape for parallel surfaces under unidirectional and bidirectional sliding. *Tribology International* 82, 1-11.

Shi, L., Y. Zhang and S. Chen (2019). Comparative research on gas seal performance textured with microgrooves and microdimples. *Journal of the Brazilian Society of Mechanical Sciences and Engineering* 41(7), 1-10.

Singh, N. and R. K. Awasthi (2021). Influence of texture geometries on the performance parameters of hydrodynamic journal bearing. *Proceedings of the Institution of Mechanical Engineers, Part J: Journal of Engineering Tribology* 235(10), 56-72.

Sun, X., P. Song and X. Hu (2021). Cross-scale flow field analysis of sealing chamber and end face considering the CO_2 real gas effect. *Journal of Applied Fluid Mechanics* 14(4), 979-991.

Tala-Ighil, N. and M. Fillon (2015). A numerical investigation of both thermal and texturing surface effects on the journal bearings static characteristics. *Tribology International* 90, 228-239.

Tibos, S. M., J. A. Teixeira and C. Georgakis (2017). Investigation of effective groove types for a film riding seal. *Journal of Engineering for Gas Turbines and Power* 139(7), 2503-2511.

Wang, T., W. Huang and X. Liu (2014). Experimental study of two-phase mechanical face seals with laser surface texturing. *Tribology International* 72, 90-97.

Wang, X., M. Khonsari and S. Li (2019). Experimental verification of textured mechanical seal designed using multi-objective optimization. *Industrial Lubrication and Tribology* 71(6), 766-771.

Wang, X., L. Shi and Q. Dai (2018). Multi-objective optimization on dimple shapes for gas face seals. *Tribology International* 123, 216-223.

Xie, J., C. Ma and S. Bai (2020). Thermo-distortion characteristics of spiral groove gas face seal at high temperature. *Numerical Heat Transfer Fundamentals* 77(3), 242-256.

Yang, X., X. D. Peng and X. K. Meng (2019). Thermo-elasto-hydrodynamic analysis of triangular textured mechanical face seals. *Journal of Zhejiang University-SCIENCE A* 20(11), 864-881.

Zhang, K., W. L. Li and J. Li (2011). Electromagnetic Interference's Effect on the Performance of Electro-Hydraulic Control System. *Applied Mechanics and Materials* 44-47, 1218-1222.